ORNL/FEDC-85/5
Dist. Category UC-20 c,d

ORNL/FEDC--85/5

DE86 007884

Fusion Energy Division

INITIAL ASSESSMENTS OF IGNITION SPHERICAL TORUS

Y-K. M. Peng, S. K. Borowski, G. T. Bussell, G. R. Dalton, G. E. Gorker, J. R. Haines, W. R. Hamilton, S. S. Kalsi, V. D. Lee, J. B. Miller, R. L. Reid, E. W. Riemer, E. C. Selcow, and D. J. Strickler

Fusion Engineering Design Center

Date Published - December 1985

Prepared by the
OAK RIDGE NATIONAL LABORATORY
Oak Ridge, Tennessee 37831
operated by
MARTIN MARIETTA ENERGY SYSTEMS, INC.
for the
U.S. DEPARTMENT OF ENERGY
Under Contract No. DE-AC05-84OR21400

CONTENTS

ABSTRACT

Initial assessments of ignition spherical tori suggest that they can be highly cost effective and exceptionally small in unit size. Assuming advanced methods of current drive to ramp up the plasma current (e.g., via lower hybrid wave at modest plasma densities and temperatures), the inductive solenoid can largely be eliminated. Given the uncertainties in plasma energy confinement times and the effects of strong paramagnetism on plasma pressure, and allowing for the possible use of high-strength copper alloys (e.g., C-17510, Cu-Ni-Be alloy), ignition spherical tori with a 50-s burn are estimated to have major radii ranging from 1.0 to 1.6 m, aspect ratios from 1.4 to 1.7, vacuum toroidal fields from 2 to 3 T, plasma currents from 10 to 19 MA, and fusion power from 50 to 300 MW. Because of its modest field strength and simple poloidal field coil configuration, only conventional engineering approaches are needed in the design. A free-standing toroidal field coil/vacuum vessel structure is assessed to be feasible and relatively independent of the shield structure and the poloidal field coils. This exceptionally simple configuration depends significantly, however, on practical fabrication approaches of the center conductor post, about which there is presently little experience.

1. SUMMARY AND DISCUSSION

An initial assessment of ignition spherical torus[1] (IST) has been completed. The purpose of this study is to quantify the potential and the challenges of an IST, to characterize its critical issues, and to highlight its data base needs. An IST is to achieve ignition for pulse lengths of the order of tens of seconds with at least the minimum number of cycles sufficient to demonstrate repeatability of results and to accomplish lowest overall cost. The major physics assumptions of an IST include:[2,3]

1. critical beta scaling proposed by Troyon,[4] with $\beta_c = 0.035\ I\ (MA)/a\ (m)\ B_0\ (T)$ and $\beta_{DT} = 0.77\beta_c$;
2. lower hybrid current ramp-up[5,6] with inductive assist only from vertical field (VF) coils (Sect. 2.1) and some plasma current decay during plasma heating, ignition, and burn, lasting for tens of seconds (a time scale much shorter than the resistive decay time of the burning plasma);
3. plasma current determined by free-boundary magnetohydrodynamic (MHD) equilibrium calculations, taking advantage of the natural elongation at low aspect ratios[2] (Sect. 2.2);
4. paramagnetism as exhibited by the plasma enhancement of the toroidal field over the externally applied field at the plasma axis, B/B_0 (Sect. 2.2);
5. energy confinement scalings, including the options of Mirnov[7] and neo-Alcator[8] (Sect. 2.4); and
6. plasma density below the Murakami limit,[9] $n\ (cm^{-3}) \leq 10^{14}\ B\ (T)/R\ (m)$, where R is the major radius.

Because of the anticipated modest field related to this concept, only conventional engineering assumptions are used in this study, with one exception: the option of using high-strength copper alloy C-17510 (Cu-Ni-Be)[10] in the center conductor post (Sects. 4.3 and 4.4) to allow for a highly compact IST and for more objective comparison with the IGNITOR class[11] of short-pulse ignition tokamaks. Otherwise, the

engineering and costing approaches are in accordance with the recent Toroidal Fusion Core Experiment (TFCX) practices.[12]

The major results of this study include the following.

1. A nominal IST with conventional coil current density (about 3.3 kA/cm^2) is estimated to have a vacuum toroidal field B_0 = 2 T at a major radius R = 1.6 m, a minor radius a = 1.0 m, a toroidal field coil current I_c = 16.2 MA, a plasma current I_p = 14 MA, a fusion power P_{DT} = 55 MW, and an ignition margin (based on Mirnov scaling) C_{ig} = 1.0 (see Table 1.1). The estimated constructed cost of the IST project ready for operation at an initially undeveloped site is $573 million in 1984 dollars (see Table 1.2). The total direct cost of the nuclear island is estimated to be $119 million. The major parameters of this benchmark case are provided in Table 1.3. Based on neo-Alcator scaling, C_{ig} for this device would become 0.27.
2. The impact of using high-strength copper alloy for the center conductor is to permit a highly compact IST with B_0 = 3 T, R = 1.0 m, a = 0.61 m, I_c = 15.1 MA, I_p = 11.9 MA, C_{ig} (Mirnov) = 1.0, and P_{DT} = 56 MW (see Table 1.1). The direct cost of the nuclear island can then be reduced by about $20 million, while the total direct cost is reduced by about $30 million.
3. The plasma paramagnetism is shown to increase strongly when the aspect ratio is decreased to less than 2.5 and when the plasma elongation is increased to and beyond 2.0. The ratio B/B_0 has a range between 1.5 and 2.3 at an aspect ratio of 1.6 when the plasma is elongated from 1.9 to 3.0. The impact of such strong paramagnetism is to allow for an IST with B_0 = 2 T, R = 1.1 m, and a = 0.67 m to have C_{ig} (neo-Alcator) = 1.4 (see Table 1.1). The application of the plasma-enhanced field in the plasma scaling laws is currently lacking in data base. When this possible effect of paramagnetism is not included, C_{ig} is smaller by roughly a factor of 4, assuming neo-Alcator scaling.
4. By combining the center conductor engineering design trade-off with the IST parameter space trade-off, it is determined that the use of the C-17510 alloy permits feasible IST designs with current density

Table 1.1. Major parameters of typical ignition spherical tokamaks
(Wall thickness Δ = 0.11 m and a scrapeoff of Δ_{s-o} = 0.1 a)

Parameters	Nominal TF coils	High-tech TF coils	Paramagnetic elongated plasma
B_0, T	2.0	3.0	2.0
B/B_0	1.7	1.7	2.3
J_c, kA/cm^2	3.3	10.0	7.0
κ	2.0	2.0	3.0
R, m	1.6	1.0	1.07
a, m	1.0	0.61	0.67
R_{TFc}, m	0.40	0.22	0.21
I_{TFc}, MA	16.2	15.1	10.7
I_p, MA	14.0	11.9	18.9
β_c	0.24 (0.14)[a]	0.23 (0.14)	0.49 (0.21)
n_{DT}, 10^{14}/cm^3	0.96 (1.6)	2.0 (3.4)	1.9 (4.4)
P_{DT}, MW	55.0 (160)	56.0 (160)	76 (404)
W_L, MW/m^2	0.26 (0.77)	0.69 (2.0)	1.5 (7.9)
P_{RU}, MW[b]	8.0	5.0	6.0
C_{ig}(Mirnov)	1.0 (2.0)	1.0 (1.9)	1.1 (3.1)
C_{ig}(neo-Alcator)	0.27 (0.73)	0.22 (0.73)	0.33 (1.4)

[a]The parameters in parentheses reflect the impact of switching from B_{t0} to B_t in the beta limit according to Troyon.[4]

[b]For a current ramp-up time of 50 s.

Table 1.2. Nominal IST cost summary

Account title		Cost (millions of 1984 dollars)	
Structures and site facilities			42.4
Reactor plant equipment			
Reactor systems			
Shielding	11.8		
Structure	28.9		
Energy, particle removal	15.4		
Total reactor systems		56.1[a]	
Magnet systems			
TF magnets	19.2		
PF magnets	37.6		
Total magnet systems		56.8[a]	
Vacuum systems		8.2[a]	
Power injection systems		19.7	
Power conditioning systems		39.6	
Heat transport systems		11.4	
Fuel handling systems		5.8	
I&C		31.7	
Maintenance equipment		28.7	
Total reactor plant equipment			258.0
Electric plant equipment			27.0
Miscellaneous plant equipment			7.3
Heat rejection system			4.1
Total direct cost			338.8
Total indirect cost			101.7
Contingency			132.1
Total constructed cost			572.6

[a] Component costs constituting the nuclear island.

Table 1.3. Reference parameters for a nominal IST

Description	Value
Geometry	
Major radius R_0	1.62 m
Plasma radius a	1.01 m
Plasma elongation κ	2.0
Aspect ratio A	1.60
Scrapeoff layer	0.10 m
Distance from scrape-off to conductor post	0.11 m
Plasma	
Average ion temperature $\langle T_i \rangle$	20 (10) keV
Safety factor (edge) q (flux surface average)	2.4
Effective charge (during burn) Z_{eff}	1.5
TF ripple (peak-to-average), edge	TBD
Plasma current I_p	14.0 MA
Average electron density $\langle n_e \rangle$	0.62 (1.25) $\times 10^{14}$ cm^{-3}
Average DT density $\langle n_{DT} \rangle$	0.44 (0.88) $\times 10^{14}$ cm^{-3}
Epsilon beta poloidal $\varepsilon\beta_p$	0.20
Total beta $\langle \beta_c \rangle$	24.3%
DT beta $\langle \beta_{DT} \rangle$	18.7%
Toroidal field at major radius B_0	2.0 T
Q	Ignited
Operating Mode	
Maximum burn time t_{burn}	50 s
Average burn time t_{bave}	20 s
Fusion power P_{fus}	50 (55) MW
Cumulative DT burn time	2×10^4 s
Years of operation	10

Table 1.3. (continued)

Description	Value
First wall - vacuum vessel	
Coolant	H_2O
Average neutron wall load at plasma edge	0.41 MW/m^2
Average neutron wall load at first wall	0.26 MW/m^2
Average thermal wall load	0.03 MW/m^2
First wall/vacuum vessel thickness	0.10 m
Shield	
Inboard shield thickness	None
Dose rate to TF coil insulation	110^{10} rad
Time after shutdown to permit pesonnel access (2.5 mrem/h)	36 h
Outboard shield thickness (90% water, 10% stainless steel)	2.50 m
Maximum structure temperature	200°C
Vacuum	
Initial base pressure	10^{-7} torr
Preshot base pressure	10^{-5} torr
Postshot base pressure	3×10^{-4} torr
Pressure at duct inlet during burn	10^{-2} torr
TF coils	
Number	36
Peak design field at winding	8.1 T
Conductor current density	3250 A/cm^2
PF coils	
Total flux capability	9.44 Wb
EF flux	9.44 Wb
Total maximum ampere-turns	11.61 MAT
Total maximum EF ampere-turns	11.61 MAT
Conductor winding pack current density	1500 A/cm^2

Table 1.3 continued

Description	Value
Current ramp-up	
Lower hybrid wave	
Rise time	50 s
Power	8 MW
Frequency	0.564 GHz
Bulk heating	
Lower hybrid wave	
Time	10 s
Power	8 MW
Frequency	1.325 GHz

J_c as high as 11 kA/cm^2. The resulting design remains within the stress limits of the alloy conductor, cooled with high-velocity pressurized water in a compact IST at a field of 3 T.

5. An IST configuration is arrived at which features internal restraining and supporting structures to allow the toroidal field (TF) configuration to be essentially free-standing (Fig. 1.1). This approach has high potential in decoupling the torus from the shield structure, contributes to minimizing the "disposal" portion of the nuclear island, and eases maintenance without significantly compromising the need to achieve very small aspect ratios.

The results of this study, although preliminary, indicate the high potential of the spherical torus concept in permitting compact ignition at modest field. The prevailing confinement and beta scaling laws, while relatively secure in their application to large tokamaks with conventional aspect ratios, yield predictions that diverge by an order of magnitude in spherical tori. A concrete physics data base is needed before the potentials of the spherical tori can be quantified with more certainty.

2. PLASMA ASSESSMENTS

2.1 LOWER HYBRID CURRENT RAMP-UP REQUIREMENTS

The elimination of induction coils in a spherical tokamak is made plausible by the use of lower hybrid current ramp-up, which is chosen here because of the recent success in Princeton Large Torus (PLT) current drive experiments.[6] The subsequent success in theoretical modeling by Fisch[5] has allowed a relatively straightforward application to IST. By maintaining the observed velocity scaling, 6 $V_{TH} = V_R = c/4$ (V_{TH}, V_R, and c being the thermal, runaway, and light velocities, respectively), and by employing a similar spectrum of the parallel phase velocities with U ($= V_{phase}/V_R$) = 1.25, an energy conversion efficiency from rf to poloidal field of about 25% (similar to the PLT results) can be assumed. The corresponding plasma density range and temperature are

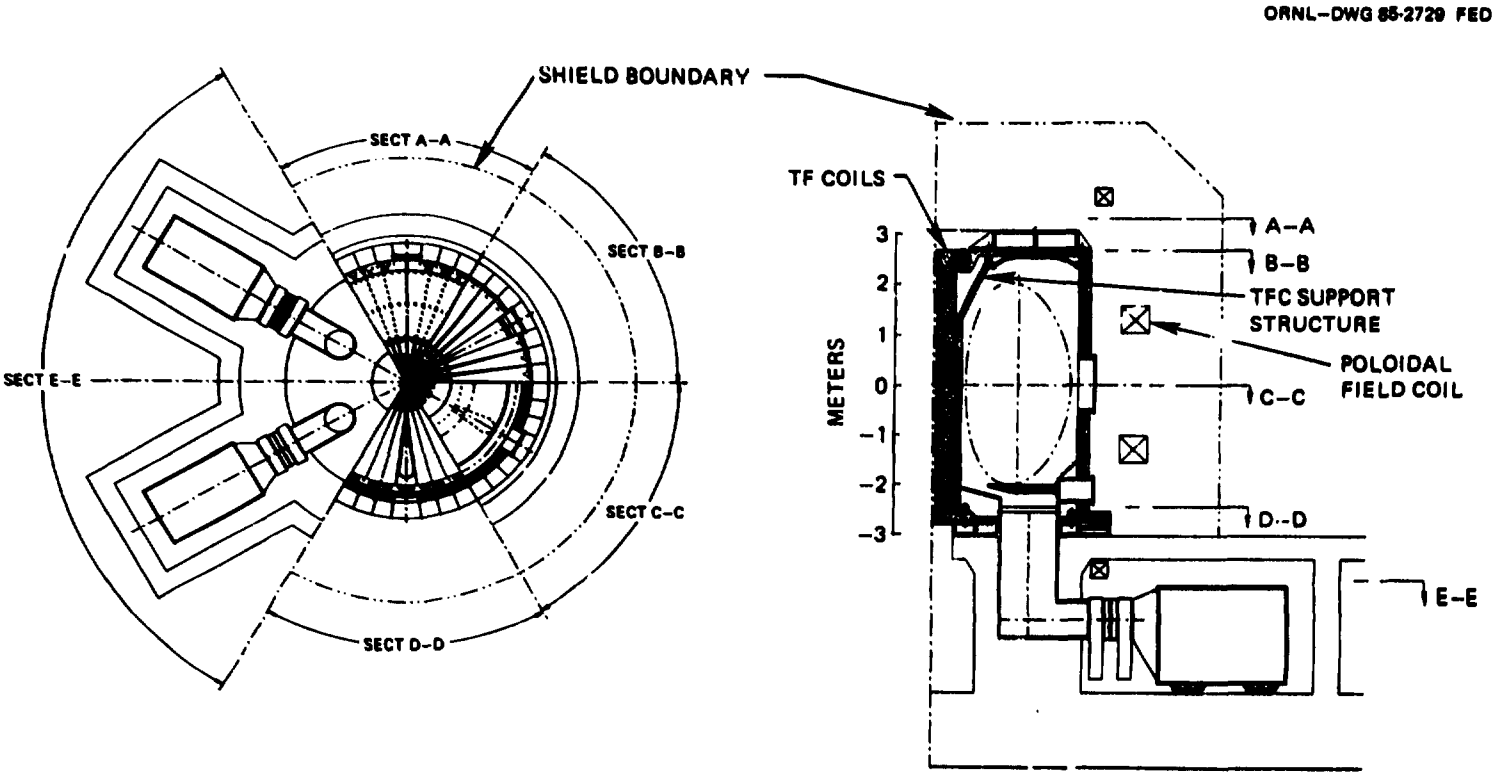

Fig. 1.1. Plan and elevation views of an IST.

estimated to be 2 to 4.4 × 10^{12} cm^{-3} and 1 keV, respectively. The required rf power launched into the plasma is estimated to be about 8 MW at 564 MHz for an IST with R = 1.5 m, B_0 = 2 T, I_p = 14 MA, leading to a ramp-up time of 55 s. With the same power at 838 MHz, the ramp-up time decreases to 20 s for an IST using a high-technology TF coil (J_c = 10 kA/cm^2) with R = 0.82 m, B_0 = 3 T, I_p = 11.5 MA. Additional parameters used in this assessment can be found in Table 2.1.

2.2 SCALING OF POLOIDAL FIELD COIL CURRENTS WITH ASPECT RATIO

Free-boundary MHD equilibrium studies were performed for elongations that increase from 1.62 at an aspect ratio of 4.0 to the natural elongation of nearly 2.0 at an aspect ratio of 1.5. Only a pair of VF coils and a pair of shaping field (SF) coils at a distance twice the minor radius from the plasma are assumed, as depicted in Fig. 2.1. In these calculations, the plasma beta is set by $0.04I_p/(aB_0)$, q(axis) = 1.0, and q(edge) = 2.4. The results are plotted in Fig. 2.2, showing that, while I_{VF}/I_p remains essentially constant, I_{SF}/I_p decreases dramatically as the aspect ratio is decreased from 4.0 to 1.5. Also plotted are the total relative ampere-turns of the poloidal field and the toroidal field coils, $\Sigma\ |I_{PF}|/I_p$ and I_{TF}/I_p, respectively, showing similar reductions. This dependence of the coil currents is expected to reduce the cost of a fusion spherical torus, such as IST.

2.3 THE EFFECTS OF ENHANCED ELONGATION AND PARAMAGNETISM

The plasma enhancement of the toroidal field, B/B_0, at the tokamak plasma major radius (defined here as paramagnetism) increases as the aspect ratio is reduced and as the plasma elongation is increased. For the range of para-meters of interest to spherical tokamaks, these dependences are calculated and shown in Fig. 2.3. The figure also shows that the natural elongation increases as the aspect ratio is reduced. The use of plasma-enhanced field in the beta and the confinement scaling laws, subject to future experimental verification, would lead to increased plasma pressure and performance. These effects are used in

Table 2.1. IST I_p ramp-up parameters

(Values assuming P_{RF} = 8 MW, conversion efficiency of 25%,[a] $V_R = c/4$, $V_{TH} = c/24$, and $V_{ph} = 1.25\ V_R$, with A = 1.57, κ = 2.0, T_e[b] = 1 keV, q_ψ = 2.4, and ℓ_i = 0.7. τ_{RU} is the estimated ramp-up time of plasma current.)

	R_0		
	1.50 m	0.978 m	0.823 m
a, m	0.952	0.623	0.523
I_p, MA	14.1	12.2	11.5
B_T, T	2.0	2.65	3.0
L_p, μH	1.0	0.656	0.552
L_pI_p, V-s	14.1	8.0	6.35
E_b,[c] V/m	2.74×10^{-2}	4.85×10^{-2}	6.12×10^{-2}
$\bar{n}$,[c] m^{-3}	2.0×10^{18}	3.50×10^{18}	4.4×10^{18}
$n_\parallel \beta$[d] = c/V_{ph}		$n_\parallel = 3.2$ ($\beta = 1$)	
		$n_\parallel = 4.5$ ($\beta = 1.4$)	
$n_\parallel$[e] ($\beta \sim 1$)		$2.0 \lesssim n_\parallel \lesssim 8.0$	
τ_{RU}, s	55	27	20
f_{LH},[f] MHz	564	746	838

[a] 25% efficiency obtained for U (= V_{ph}/V_R) ≈1.25.

[b] The ability to maintain T_e ≈ 1 keV with multimegawatt rf levels is an area of concern.

[c] Electric field and density values required to maintain $V_R = c/4$.

[d] Factor to account for upshift in $n_\parallel$ for waves in plasma.

[e] $n_\parallel$ - spectrum range for $0.5 \lesssim \mu \lesssim 2.0$.

[f] $f_{LH} = \omega_{LH}(0)/\pi$ with assumed parabolic density profiles.

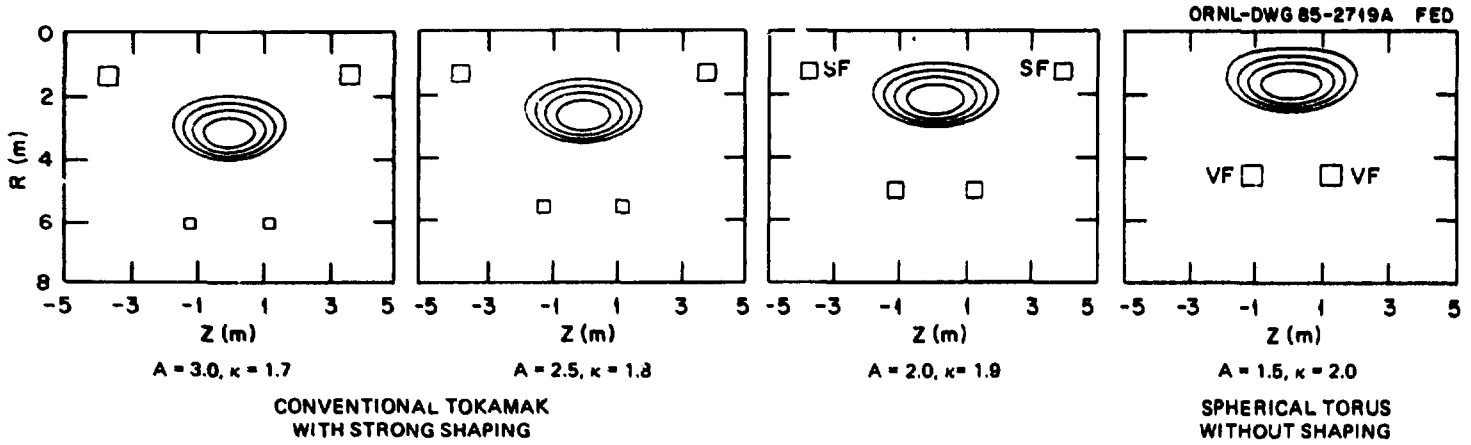

Fig. 2.1. Plasma and PF coil configurations used in the cases of Fig. 2.2.

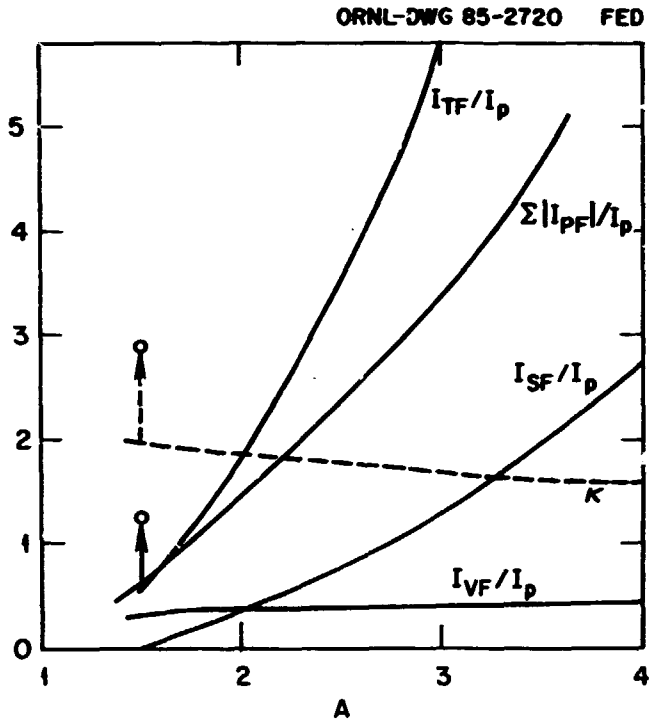

Fig. 2.2. Dependence of vertical field (VF), shaping field (SF), poloidal field (PF), and toroidal field (TF) coil ampere-turns relative to the plasma current on the aspect ratio A for the elongation indicated.

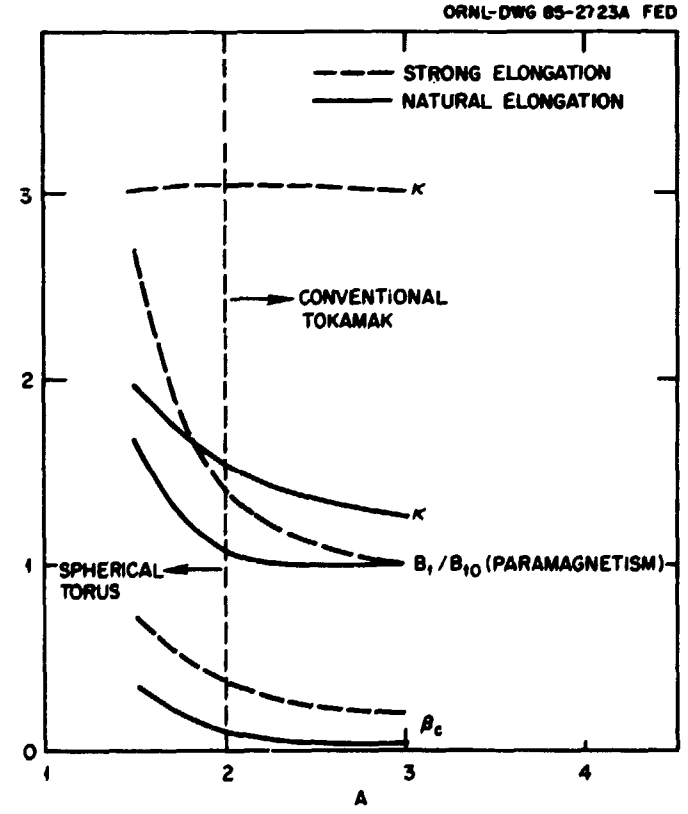

Fig. 2.3. Dependence of paramagnetism on aspect ratio and elongation.

scoping the IST size and the major parameters. Assuming the strong elongation and paramagnetism indicated in the figure and neo-Alcator scaling, an IST with $\kappa = 3.0$, $B_0 = 2$ T, $C_{ig} = 1.4$, and central conductor current density $J_c = 7$ kA/cm^2 would have $B/B_0 = 2.3$, R = 1.07 m, a = 0.67 m, $\beta_c = 0.49$ (with respect to B_0), and a fusion power near 400 MW (Table 1.1).

2.4 CONFINEMENT SCALING ASSUMPTIONS

A new physics code[13] has been developed for the Fusion Engineering Design Center (FEDC) Tokamak Systems Code. The unique features of this code include a two-fluid model of the ion-electron power balance and a comprehensive treatment of the confinement modeling. The code can generate contours of steady-state plasma operating and heating regimes for a given device showing sensitivities to various equilibrium, stability, and confinement assumptions. Results from the code show a reasonable agreement with those from the 1½-D radial transport WHIST code.[14]

In the ignition system studies performed for the spherical torus, the following specific confinement modeling assumptions were utilized: the Chang-Hinton neoclassical formulation for the ion losses[15] and the Mirnov[7] or neo-Alcator[8] empirical scaling laws for the electron losses. The global energy confinement time is given by:

$$\tau_E = \frac{R_{nt} + 1}{(R_{nt}/\tau_{Ei}) + (1/\tau_{Ee})} ,$$

where τ_{Ee} is the electron energy confinement time, which is assumed to follow the Mirnov, H-mode scaling ($\tau_{Ee} = 0.39\, \bar{a} I_p$) or the neo-Alcator scaling ($\tau_{Ee} = 0.08 n_e R^2 \bar{a} q$), with $\bar{a}$ (average minor radius) and R in meters, I_p in MA, and n_e in 10^{20} m^{-3}; τ_{Ei} is the neoclassical ion energy confinement time, given by

$$\tau_{Ei} = \frac{T_i^{1/2} B_0^2 a^2 \kappa^2 (f_\tau)}{f_i (6.5 \times 10^{-22}) K Z_{eff} A^{3/2} n_e q^2} ;$$

and we have defined $R_{nt} = (n_i/n_e)(T_i/T_e)$; B_0 is the vacuum toroidal field on axis in tesla; $\bar{a} = a[2\kappa^2/(1 + \kappa^2)]^{1/2}$, depicting the transport step size for concentric elliptical flux surface geometry; Z_{eff} is the effective charge; K is the large-aspect-ratio correction factor,

$$K = [0.66 + (1.88/A^{1/2}) - (1.54/A)] [1 + (1.5/A^2)] ;$$

f_τ is the factor relating χ and τ_E, which is about 3/16 for flat density and parabolic temperature profiles; and f_i is the enhancement factor reflecting anomalies in ion energy loss. In this analysis (Table 1.1), we assume $f_i = 2$, $Z_{eff} = 1.5$, $T_i = T_e = 10.0$ keV, $A = 1.6$, and $q = 2.4$.

The large plasma current in the low-aspect-ratio spherical torus results in a prediction of a significantly larger ignition margin under the Mirnov confinement scaling than under the neo-Alcator model.

3. SYSTEMS CODE TRADE-OFF STUDIES

3.1 BENCHMARK (REFERENCE) CASE

The Tokamak Systems Code has been modified from the current version[16] and used to assess the dependences of the IST on field, coil current density, and uncertainties in confinement scaling. These code modifications include the elimination of the ohmic heating (OH) solenoid and the inboard shield, the alterations to the TF coil and the shield configurations, the adjustments in the operating scenario, etc. The benchmark configuration with a major radius of 1.62 m, an aspect ratio of 1.6, and an ignition margin of 1.5 was calculated to have a direct capital cost of $402 million in 1984 dollars (with some adjustments). Approximately $72 million of this total is for the nuclear island, which includes shielding, vacuum vessel, limiters, reactor structure, TF and poloidal field (PF) magnets, and reactor vacuum equipment. The benchmark case parameters are given in Table 1.3.

When the neo-Alcator confinement scaling is applied to the benchmark case, a decrease of the ignition margin to 0.4 results if T = 10 keV (Table 1.1) and if the plasma pressure is not enhanced by plasma paramagnetism. The potential benefit of field enhancement by the spherical torus plasma is summarized in Sect. 2.3.

3.2 DEPENDENCE ON COIL CURRENT DENSITY

Trades were performed for increasing the center post current density (selected values were 3.0, 5.0, 7.5, and 10 kA/cm^2) with the results plotted in Fig. 3.1. An ignition margin of 1.5 was maintained under Mirnov scaling, and the externally applied field on axis was kept at 2.0 T. There is an increase in beta (with respect to B_0) from a minimum of 24% to a maximum of 32% as the current density increases due to a modest decrease in aspect ratio from 1.62 to 1.48. Simultaneously, there are decreases in fusion power (from a maximum of 50 MW at 3 kA/cm^2 to 42 MW at 10 kA/cm^2) and major radius (1.66 to 1.20 m). Costs for the nuclear island decreased from \$74 to \$52 million, while the total direct cost decreased by about \$30 million. The 3-kA/cm^2 machine was \$3 million more than the benchmark case; the 10-kA/cm^2 case was \$30 million less. Note that the systems code used does not have the dependence of TF coil resistivity on the coil temperature, which increases with current density. Power requirements for the coil and coil cooling equipment increase significantly as the 10-kA/cm^2 value is approached. This issue is more thoroughly addressed in Sects. 4.3 and 4.4. Also note that a dual use of lower hybrid resonance wave for current ramp-up and heating at a single frequency in the IST operating scheme was assumed in these calculations. Two separate systems with different frequencies are currently expected for these functions. The cost of the rf system does not reflect this, although the total rf power estimated is included in the estimates.

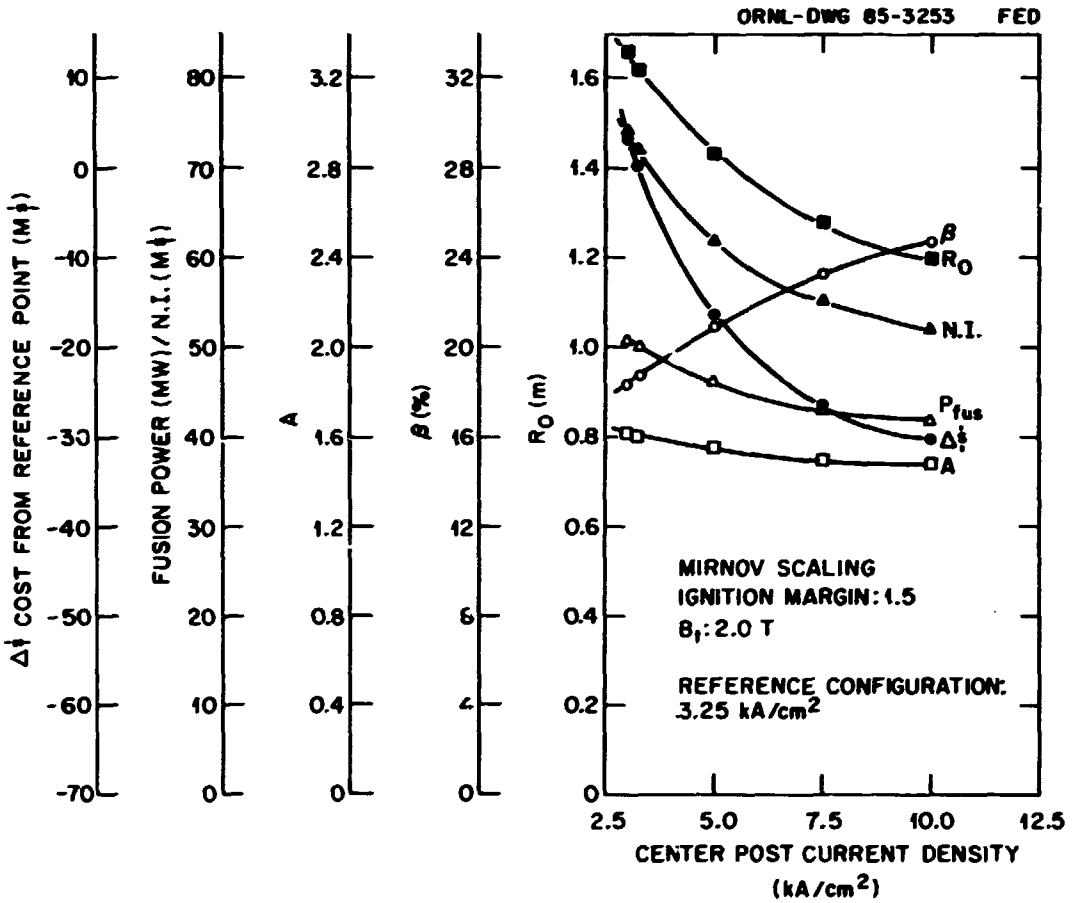

Fig. 3.1. IST trade-offs with respect to the center conductor post current density.

3.3 DEPENDENCE ON EXTERNALLY APPLIED TOROIDAL FIELD

Trades were performed by varying the field on axis from 2 to 4 T with a center post current density fixed at 10 kA/cm^2 and an ignition margin of 1.5 (Mirnov). The aspect ratio increased from 1.48 to 1.8 with B_0, as did the fusion power (42 to 60 MW). The nuclear island cost decreased from \$53 million to \$34 million; the total direct cost decreased from the benchmark case by \$30 million at 2 T and \$67 million at 4 T. Beta decreased from 32 to 18% with aspect ratio A increasing from 1.48 to 1.8 as the major radius is decreased to 0.9 m. The results are plotted in Fig. 3.2.

3.4 SENSITIVITY TO UNCERTAINTIES IN CONFINEMENT SCALING

Because of its cubic dependence in plasma size, the neo-Alcator scaling exhibits a dramatic deviation from the Mirnov scaling in confinement predictions for spherical tori. Three neo-Alcator cases were examined at 10 kA/cm^2 using an ignition margin of 1.5 and varying the vacuum field on axis (B_0) from 3 to 5 T. The trends with increasing field are similar to the preceding calculation, except that the fusion power now decreases with increasing field but at a much higher level. Relative to the case with Mirnov confinement scaling, Fig. 3.3 shows that as B_0 is increased from 3 to 5 T, R decreases from 1.8 to 1.3 m; P_{DT} decreases from 1 to 0.89 GW; β decreases from 29 to 18%; the nuclear island cost decreases from \$156 million to \$83 million; but A increases from 1.42 to 1.64. These results show a dramatic contrast with the IST parameters when the plasma-enhanced B field, rather than the externally applied field (B_0), is used in the confinement and beta scalings. As shown in Table 1.1, this assumption would lead to R ≈ 1.1 m and P_{DT} ≈ 0.4 GW.

4. ENGINEERING ASSESSMENTS

4.1 REFERENCE CONFIGURATION

Elevation and plan views of the reference IST are shown in Figs. 4.1 and 4.2, respectively, corresponding to the major plasma parameters

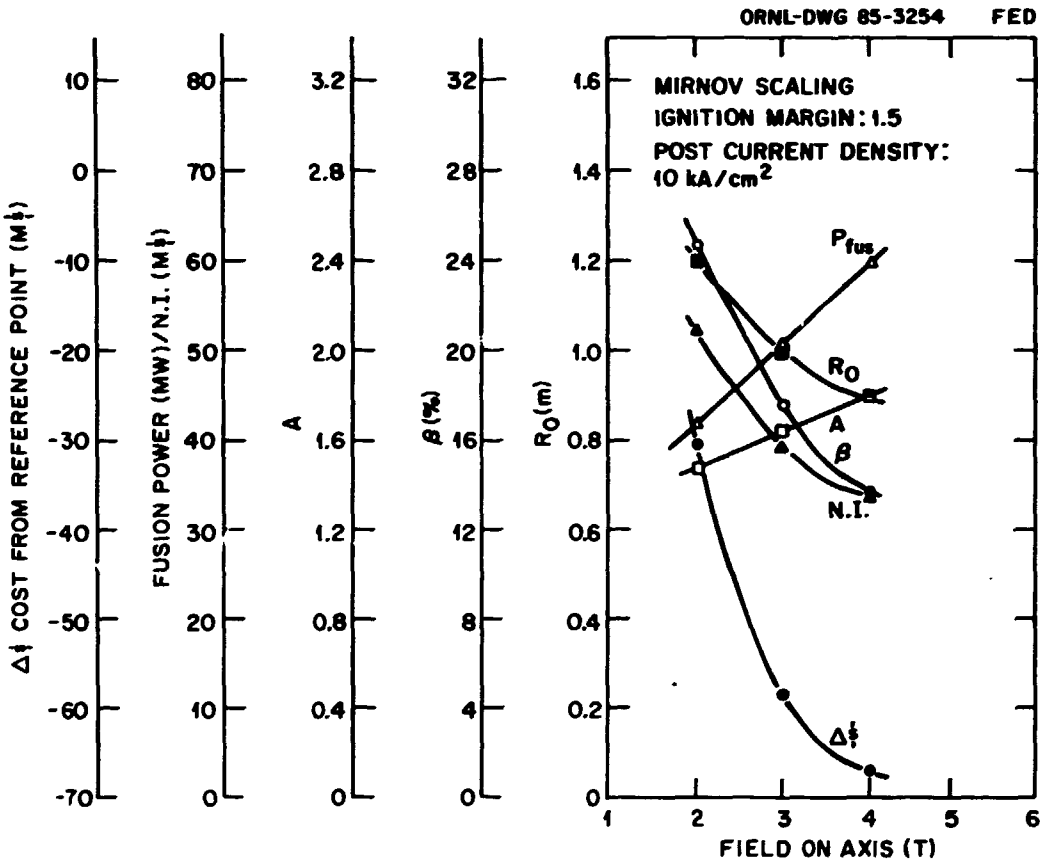

Fig. 3.2. IST trade-offs with respect to B_0, assuming Mirnov scaling.

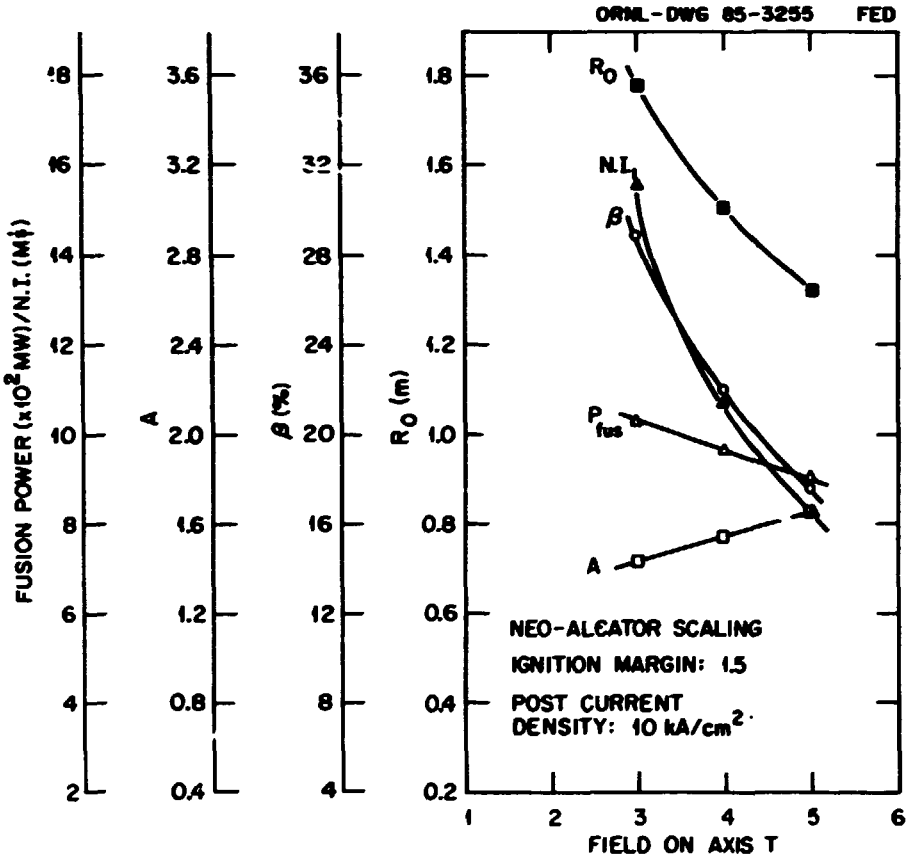

Fig. 3.3. IST trade-offs with respect to B_0, assuming neo-Alcator scaling.

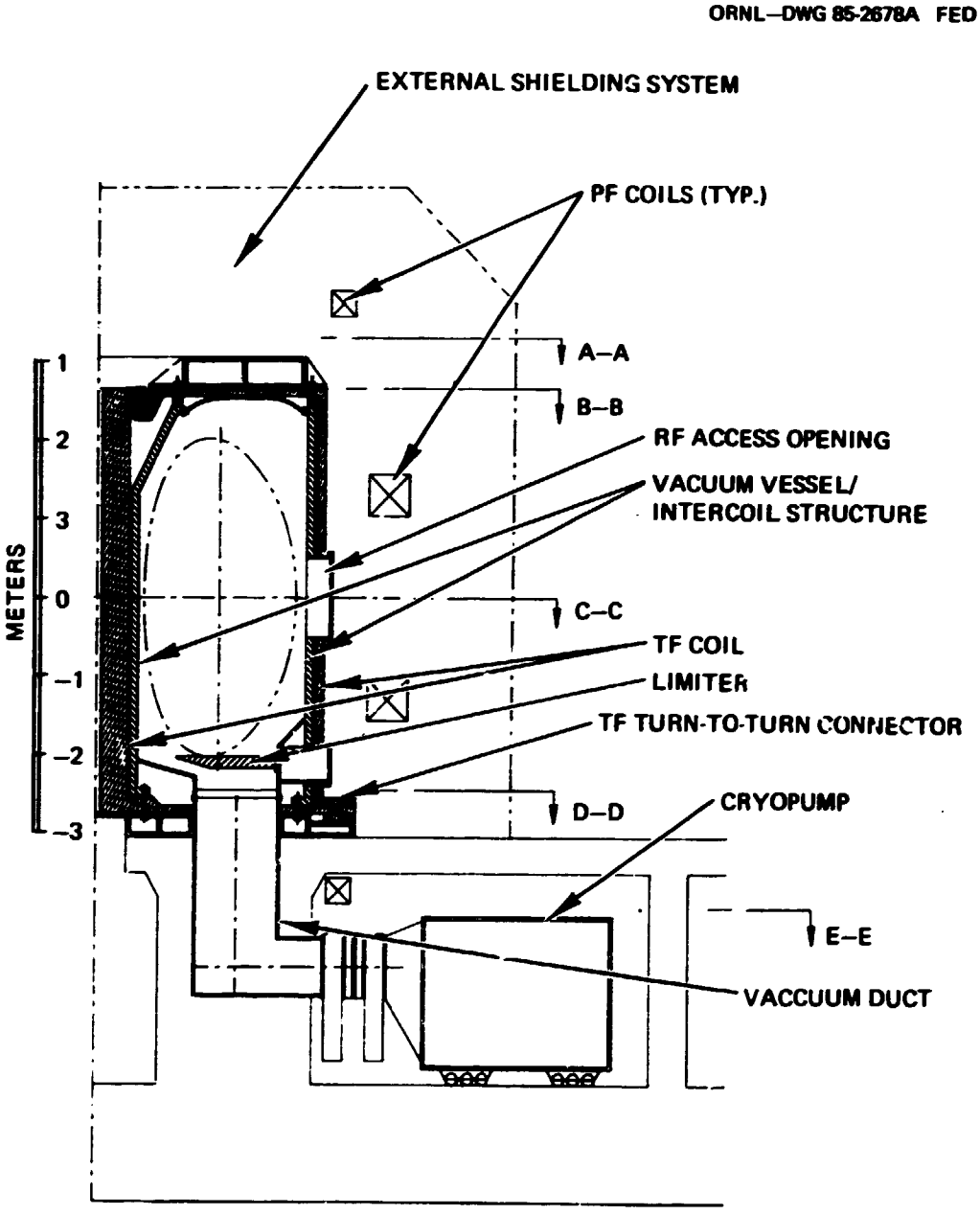

Fig. 4.1. Elevation view of the nominal IST.

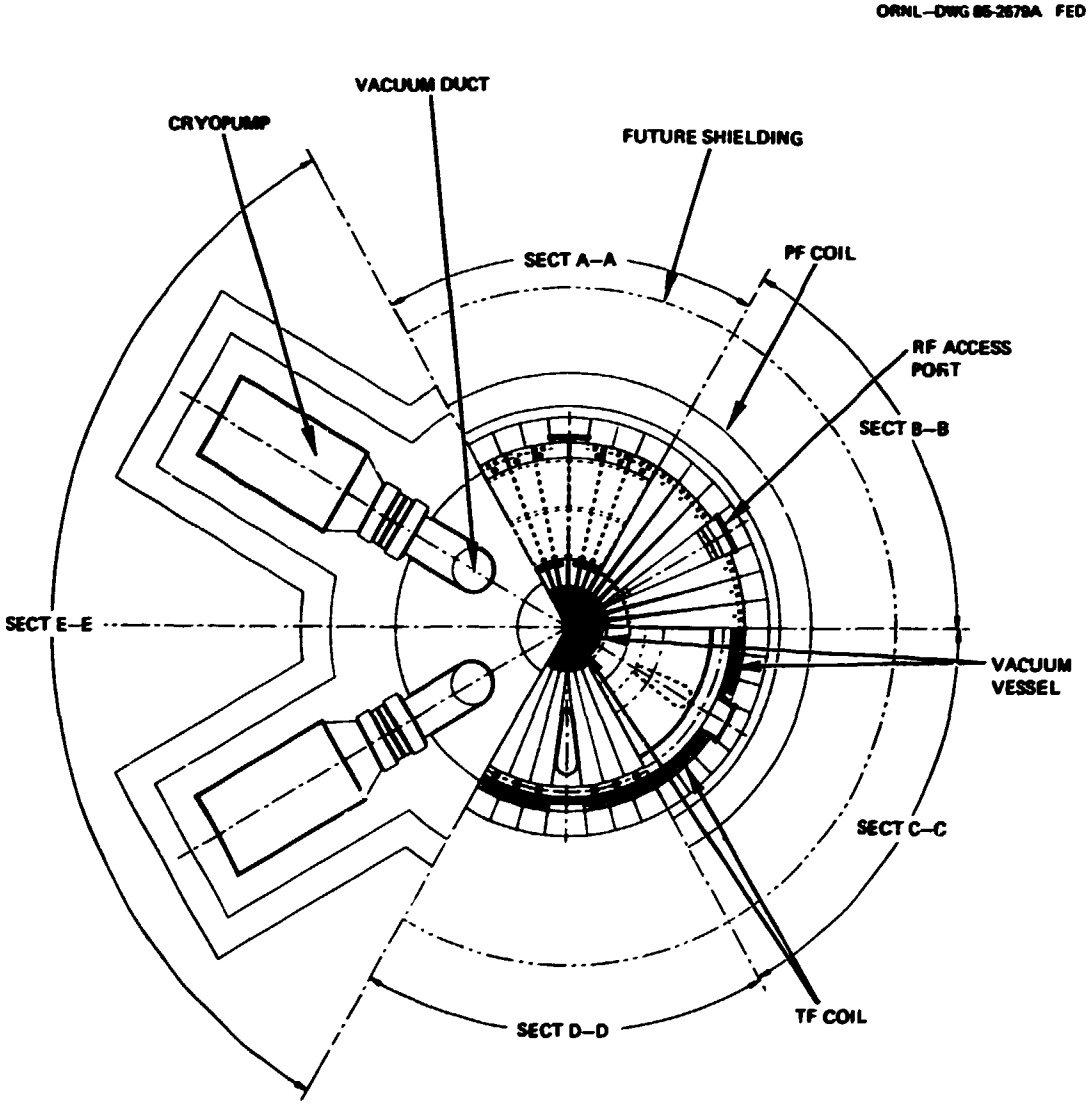

Fig. 4.2. Plan view of the nominal IST.

listed in Table 4.1. The primary features of the reference concept are: (1) a 36-turn TF coil system connected in series with the top leg of each coil, which is removable for access, (2) a thick-wall vacuum vessel/first-wall structure, which also functions as intercoil structure, and (3) a 2.5-m-thick external shielding system of water in steel tanks, which can be added by phased construction prior to deuterium-tritium (DT) operation.

The TF coils in this concept are rectangular in shape with the center leg having wedged TF turns. In the radial build, the center leg begins at a radius of 5 cm and ends on a radius of 40 cm. The toroidal wedge angle is 10°. The average current density is 3 kA/cm^2.

The outer leg of each TF coil turn has a toroidal thickness of 40 cm and a radial thickness of 10 cm. The current density in the outer leg is about 1 kA/cm^2. The 40-cm width for each of the 36 TF coil outer legs arranged in a toroidal array allows access openings (60 cm in the toroidal direction) at six equally spaced locations. Access openings at midplane are for lower hybrid rf heating units. Access openings at the limiter elevation are provided for coolant and attachment connections.

The top and outer legs of the TF coil are removable. The center leg mates with the top leg by means of an eight-finger lap joint with two bolts. The top leg mates with the outer leg by means of a bolted lap joint. Turn-to-turn electrical connection occurs between the outer leg and the bottom leg of the adjacent turn at floor level. The turn-to-turn connector lies on top of the inlet electrical bus, which makes a full toroidal loop around the machine prior to mating with the bottom leg of the first turn. Current in the turn-to-turn connector flows in the opposite direction to the current flowing in the inlet bus, cancelling the error fields generated. The total TF coil weight is estimated to be 150,000 kg (330,000 lb).

The inner and outer rings of the vacuum vessel function as TF intercoil structures for both in-plane and out-of-plane TF coil loads. The lid of the vacuum vessel is removable for access to the plasma chamber.

This 36-turn concept has two distinct advantages over concepts with fewer turns (such as 12). First, the thin center legs of the TF coil allow the entire coil to be made by machining copper plate or bar stock,

Table 4.1. Major plasma parameters for IST reference configuration

Major radius, m	1.62
Minor radius, m	1.01
Field on axis, T	2.0
Elongation	2.0
Plasma current, MA	14.0
Current in center legs, MA	14.8
Average beta, %	23
Safety factor	2.4
Fusion power, MW	52
Average neutron wall load, MW/m^2	0.45

while the 12-turn center legs require large castings. Second, the power supply cost for the 36-turn concept is substantially less than that for the 12-turn concept (33% less for an ac/dc power converter and 20% less for a storage battery system, see Sect. 4.5). The design challenges in this concept are essentially the same as for the 12-turn concept, and involve the cooling of the thin, high-current-density center conductors and the vacuum vessel structures.

4.2 ALTERNATE CONFIGURATIONS

4.2.1 Conventional Configuration

Elevation and plan views of the conventional configuration are shown in Fig. 4.3; its major parameters are listed in Table 4.2. The primary features of this concept are: (1) one center TF conductor with 12 discrete outer TF coil legs connected in parallel circuits, (2) a separate vacuum vessel, which also functions as a first wall, and (3) a 1.0-m-thick shield (80% steel, 20% water) between the plasma and the TF outer legs.

The center TF conductor is 8.65 m in height and has a diameter of 0.62 m. Because the current density is 4.5 kA/cm^2, the center conductor will require approximately 100 separate cooling channels. Each outer TF coil leg has a width of 0.65 m and a thickness of 0.18 m, resulting in a current density of less than 1.0 kA/cm^2. Because the outer TF coil legs are parallel circuits, each leg will require a separate power supply, providing 1.125 MA.

The key design challenges of this concept are the center conductor and the dual-function vacuum vessel/first wall. The center conductor gross weight is 24,000 kg (51,000 lb); it would be manufactured by a special, one-of-a-kind casting process. Both of these processes are close to being beyond the state of the art. The vacuum vessel/first-wall component is an actively cooled structure that must carry vacuum pressure loading as well as surface and neutronic heat loads. Intercoil structure is expected to be required to react in-plane and/or out-of-plane forces.

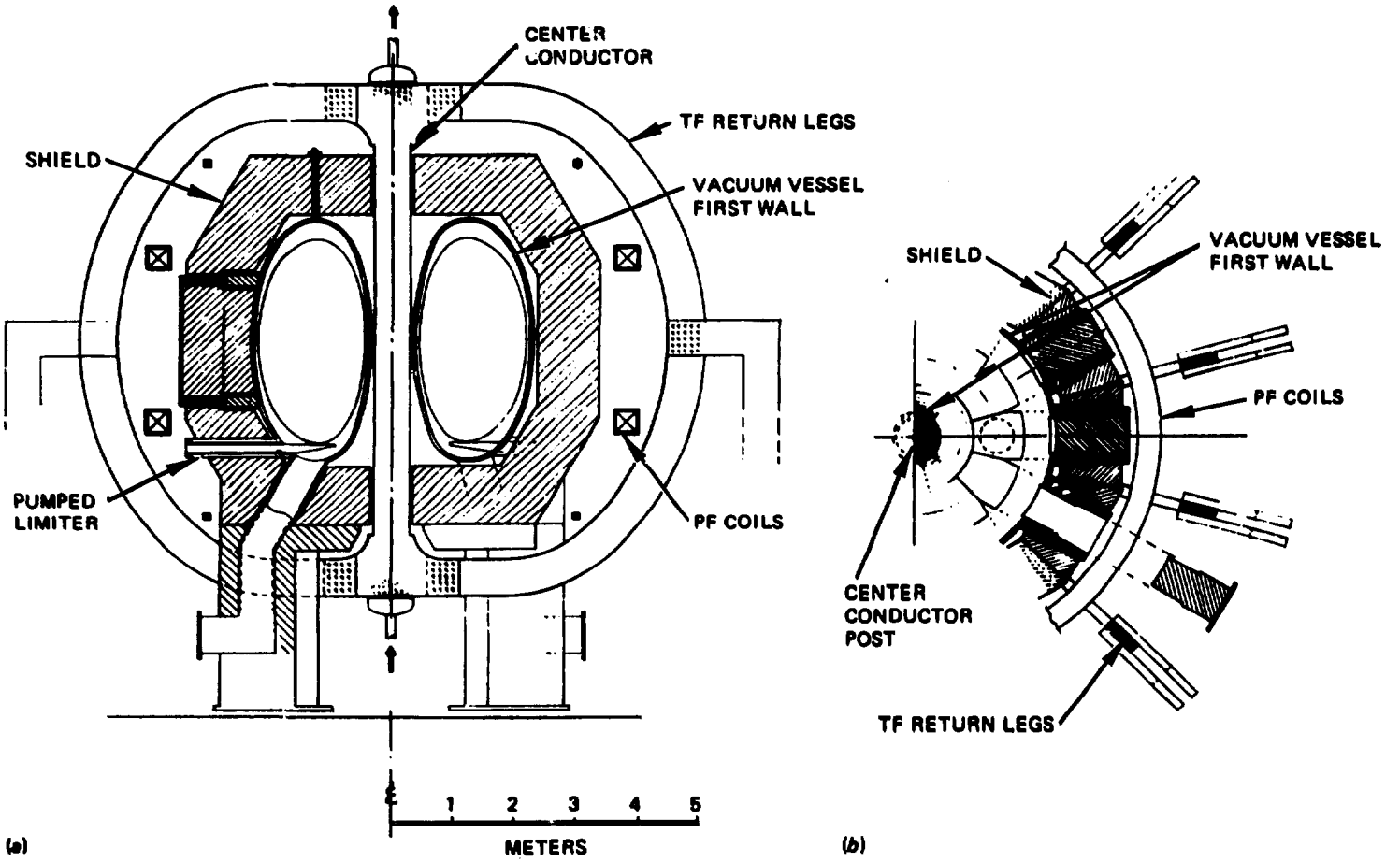

Fig. 4.3. (a) Elevation and (b) plan views of the conventional configuration.

Table 4.2. Major parameters for conventional configuration

Major radius, m	1.35
Minor radius, m	0.88
Field on axis, T	2.0
Elongation	2.0
Plasma current, MA	14.1
Current in center leg, MA	13.5
Average beta, %	26
Safety factor	2.4
Fusion power, MW	52.4
Average neutron wall load, MW/m^2	0.59

4.2.2 Configuration with 12-Turn TF Coils

Elevation and plan views of a concept with 12-turn TF coils are shown in Figs. 4.4 and 4.5, respectively, with the major plasma parameters listed in Table 4.3. The primary features of this concept are: (1) the 12 center TF conductors with 12 continuous outer TF legs connected in series circuits, (2) a separate vacuum vessel, which also functions as a first wall, and (3) a 2.5-m-thick external shielding system of water in steel tanks, enclosing the TF coil structure.

The center TF region is composed of 12 pie-shaped TF conductors, which are 5.2 m in height and have an outer radius of 0.38 m. Wedging of the pie-shaped conductors reacts in-plane centering loads of the 12 conductors. The current density of the center region is 3.0 kA/cm^2. Approximately 100 separate cooling channels will be required in the center TF region. The top, bottom, and outer TF legs each have separate cooling channel circuits. Each outer TF coil leg is 1.5 m wide and 8 cm thick, resulting in a current density of less than 1.0 kA/cm^2. Because this configuration has 12 separate TF coils in a series circuit, only one 1.15-MA power supply is required. The turn-to-turn connectors are located at the joint of the outboard and bottom legs of the TF coils where the current in the outboard leg is transferred to the bottom leg of the adjacent turn. Reaction of the in-plane and out-of-plane forces in the top, bottom, and outer legs of the TF coils is carried by the external shielding structures (steel structures for top and outer legs and concrete for bottom legs).

The key design challenges of this concept are the center TF conductors, the joint of the top and bottom TF legs to the center conductor, and the vacuum vessel/first-wall structure. Each center conductor would be manufactured by a casting process requiring 1750 kg (3850 lb) of copper. Actual joints of the top and bottom legs to the center legs require more detailed evaluation. The vacuum vessel/ first-wall structure is actively cooled and must be designed for vacuum pressure and thermal surface and neutronic heating loads. The concrete shielding system below the floor level is expected to be adequately flexible to shield the bottom region of the plasma chamber.

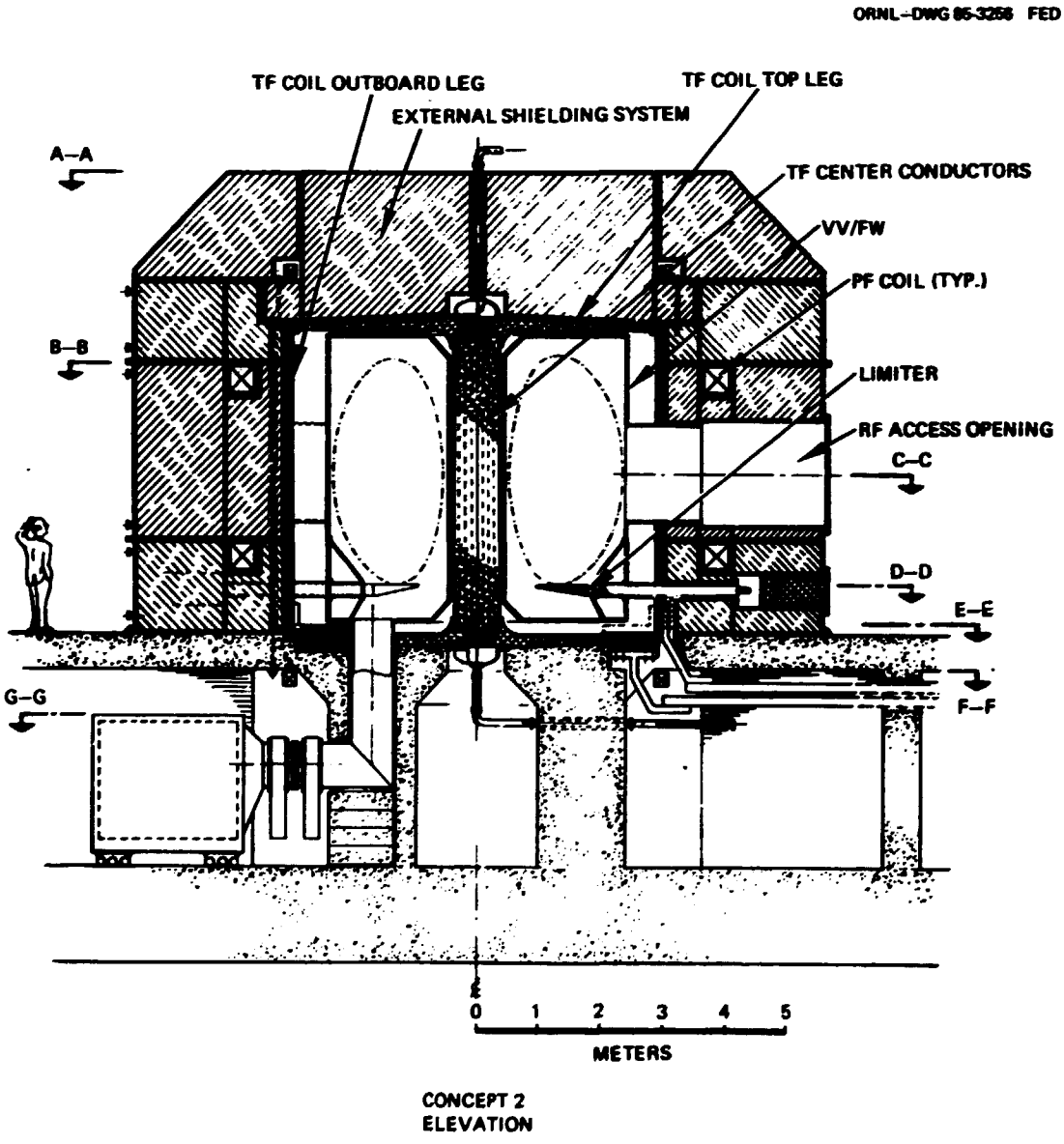

Fig. 4.4. Elevation view of alternate configuration with 12 TF coil turns.

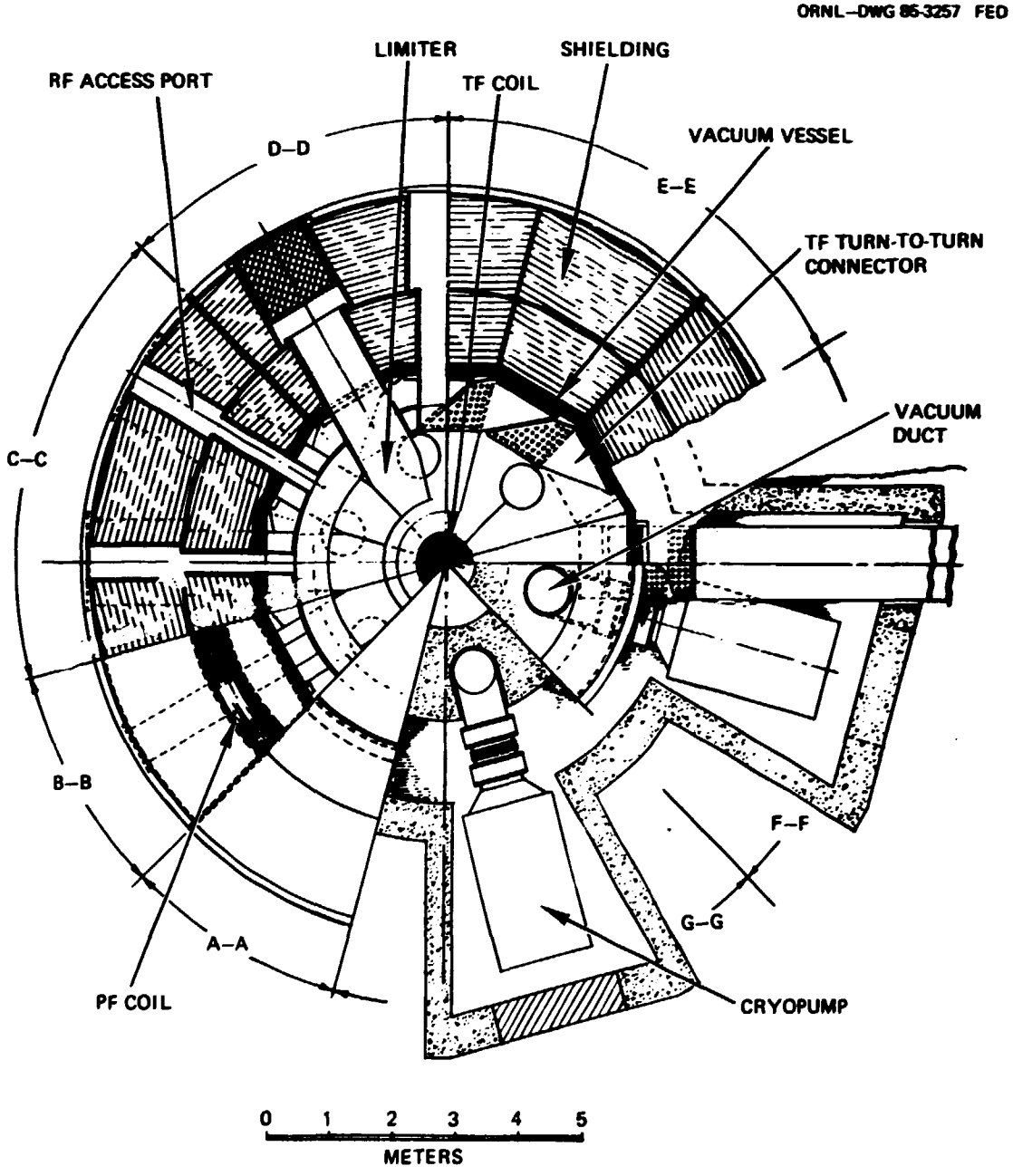

Fig. 4.5. Plan view of alternate configuration with 12 TF coil turns.

Table 4.3. Major plasma parameters for alternate configuration

Major radius, m	1.41
Minor radius, m	0.91
Field on axis, T	2.0
Elongation	2.0
Plasma current, MA	14.0
Current in center leg, MA	13.8
Average beta, %	25.5
Safety factor	2.4
Fusion power, MW	52.0
Average neutron wall load, MW/m^2	0.57

4.3 COMPARISON OF CONVENTIONAL COPPER AND HIGH-STRENGTH COPPER ALLOY TF COILS

Investigation of oxygen-free high-conductivity (OFHC) copper TF coils shows that the limiting problem is the magnetic compressive stress in the copper. If annealed copper is used, the product of current density times central leg radius, $J_c R_c$, must be kept below 10 MA/m. In the reference IST, a current density of 30 MA/m^2 in a conductor radius of 0.39 m can be satisfied by a modest 10 to 20% cold working of the copper. Other critical parameters, such as copper temperature, water velocity, and pressure drop, are estimated to be 148°C, 3.4 m/s, and 24.8 kPa, respectively, in a center conductor 3.8 m in length.

Investigation of high-strength, high-conductivity copper alloys, such as C-17510 (Cu-Ni-Be), for use in the central legs of the TF coils shows that the alloy will allow current densities as high as 10 kA/cm^2 with acceptable but challenging levels of copper temperature (327°C), water velocity (27.4 m/s), and pressure drop (2.63 MPa) in a center conductor 3.1 m in length. The compressive stress in the copper alloy is not a limiting factor in the center conductor design with $J_c R_c$ = 19 MA/m in a highly compact IST of R = 0.82 m and B_0 = 3 T. Additional parameters of the operating conditions of these center conductor posts are provided in Table 4.4.

4.4 CENTER CONDUCTOR POST

A trade-off study was performed to determine the center conductor post current density that minimizes the direct capital cost of the IST. Two materials, pure copper and a high-strength Cu-Ni-Be alloy (C-17510), were evaluated. Compressive stresses in the coil limit the current density to below 4.4 kA/cm^2 for pure copper and to 11 kA/cm^2 for the alloy, subject to effective heat removal at acceptable temperatures to maintain the strength of the copper (see Fig 4.6). Operating pure copper at the above current density limit results in a savings of $24 million compared with a device operating at the nominal current density of 3 kA/cm (see Fig. 4.7). Designing the Cu-Ni-Be alloy center

Table 4.4. Representative operating conditions of IST center conductor post

Parameters	OFHC copper	C-17510 copper
J_c, kA/cm^2	3.0	10.0
R_c, m	0.39	0.19
R, m	1.5	0.82
B_0, T	2.0	2.9
L_c, m	4.8	3.1
I_c, MA	14.3	11.5
B_c, T	7.7	12.5
Copper stress, ksi	11.1	29.6
I^2R power, MW	61	237
V_w, m/s	3.4	27.4
P_{pump}, MW	0.01	1.2
Passage radius	1.5	0.74
Cooling duct distance, cm	7.8	3.8
Pressure drop, psi	3.6	381
Inlet temperature, °C	20	20
Outlet temperature, °C	80	140
Maximum copper temperature, °C	148	327

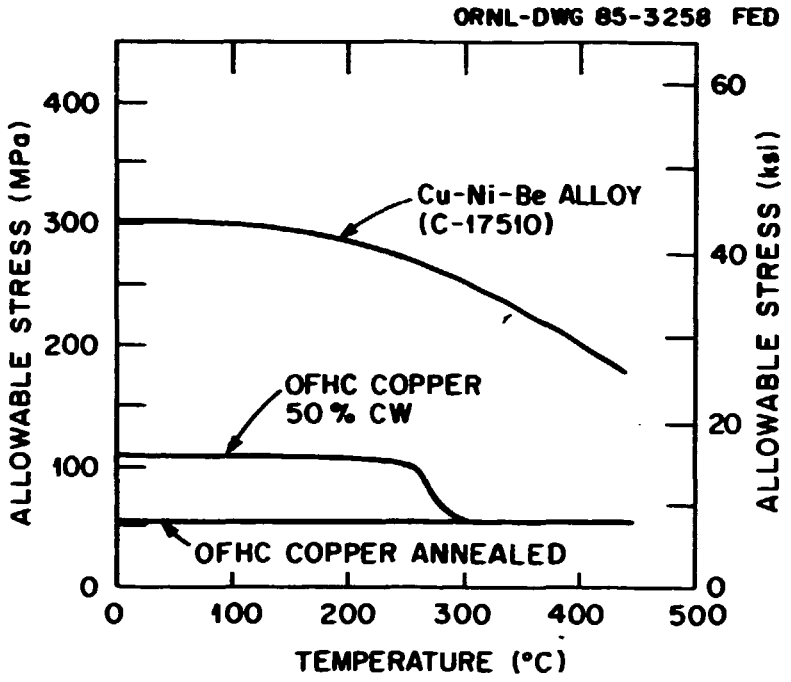

Fig. 4.6. Dependence of assumed allowable stress on temperature for the copper options considered.

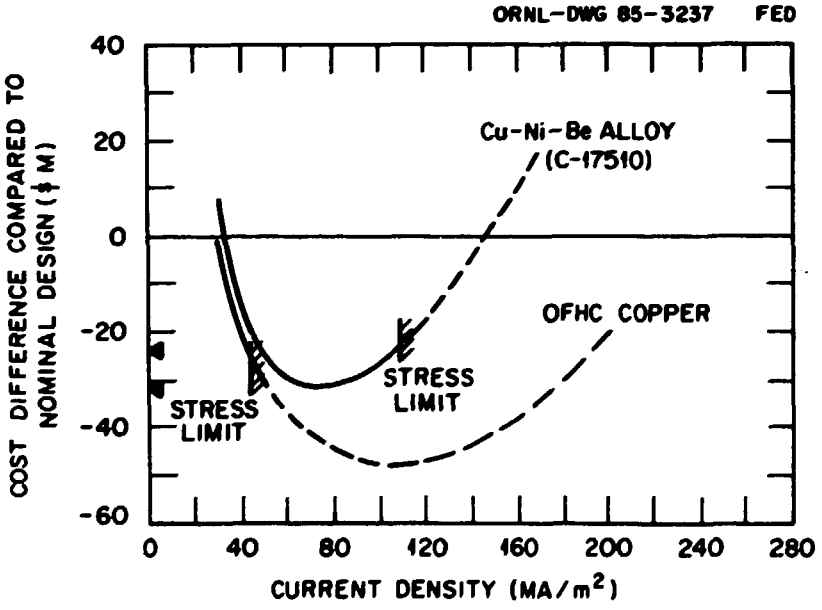

Fig. 4.7. Trade-off of IST cost with center conductor current density.

conductor post to operate at a current density of 7 kA/cm^2 would minimize the cost and save $32 million compared with the nominal device design (Fig. 4.7). These results suggest that highly compact ISTs are possible if a high-strength conductor can be used, contributing to a highly cost-effective nuclear island.

4.5 IST ELECTRICAL POWER SYSTEMS

Several alternate TF coil power conversion systems were investigated, including homopolar generators, batteries, high-current thyristor power supplies, and gas turbine flywheel generators. All of these options are estimated to be relatively costly for single-turn currents that range from 1 to 10 MA. For currents ranging from 200 to 500 kA, however, the batteries and the thyristor supplies appear to be the more economical. When the power conditioning control and maintenance equipment are included, the thyristor supplies appear to be the most economical. The best trade-off between the number of TF coil turns and power supplies occurs when the TF coils have about 36 turns.

In the case of ac helicity injection,[17,18] a silicon controlled rectifier (SCR)-controlled power factor correction of about 280 MVA reactive (MVAR) is required to accommodate a 1% current modulation at the estimated frequency of about 5 Hz. This would add about $9 million to the substation cost estimate. The total cost estimated for the electrical power systems is then $40 million based on the thyristor approach.

4.6 LOWER HYBRID CURRENT DRIVE SYSTEM

The IST assumes lower hybrid current drive (LHCD) to ramp up the plasma current to 14 MA. The plasma density and temperature during ramp-up are such that a wave-to-toroidal current efficieny of 25% is obtained. The LHCD system necessary to accomplish this can be characterized by a source frequency of 564 MHz and a launcher grill spectrum centered around N = 3.? and a width of 0.5 m. Two 0.65- by

0.56-m arrays of 2 × 12 apertures each are needed. Each aperture measures 0.03 by 0.31 m and carries a maximum of 250 kW. Adjacent apertures are phased 180° apart. Twenty-four rf sources are used to produce 12 MW, of which 8 MW are launched at the plasma edge.

4.7 INBOARD SHIELDING REQUIREMENTS

Radiation exposure limits for the spherical torus center conductor post were examined. Damage to the copper conductor and turn-to-turn insulation was considered. Based on the analysis, it is unnecessary to provide inboard shielding in the design of the IST. For a reference total DT burn time of 2×10^4 s, epoxy-fiberglass insulation is marginally acceptable. To ensure adequate insulation lifetime, polyimide fiberglass insulation is recommended.

4.8 PRECONCEPTUAL COST ESTIMATE

A preconceptual cost estimate of the IST device has been generated utilizing the FEDC computerized cost estimation spreadsheet and cost data base file.[19] This menu describes the assumptions, definitions, and methodology incorporated into the development of the IST cost estimate and presents a detailed breakdown of the projected costs. As shown in Table 2.1, the estimated total constructed cost of the IST device in mid-1984 dollars is $573 million. This includes contingency, construction of the facility at an undeveloped site, and bringing it into operation. The total direct cost of the nuclear island is estimated to be $119 million.

ACKNOWLEDGMENT

The authors would like to acknowledge the encouragement of this work by T. E. Shannon and others at the FEDC, the graphics support by M. H. Kunselman, and the preparation of the manuscript by P. A. Powell and M. E. Talley.

REFERENCES

1. Y-K. M. Peng, Spherical Torus, Compact Fusion at Low Field, ORNL/FEDC-84/7, Oak Ridge National Laboratory, January 1985.
2. Y-K. M. Peng and D. J. Strickler, "Features of Spherical Torus Plasmas," submitted to Comments Plasma Phys. Controlled Fusion.
3. Y-K. M. Peng, "Features of Spherical Torus Plasmas of Ultra-Low Aspect Ratio and Large Elongation," presented at the 12th European Conference on Controlled Fusion and Plasma Physics, September 2-6, 1985, Budapest, Hungary.
4. F. Troyon et al., Plasma Phys. Controlled Fusion 26 (1A), 209 (1984).
5. N. J. Fisch and C. F. F. Karney, Current Ramp-up with RF Waves in a Tokamak, PPPL-2132, Plasma Physics Laboratory, Princeton University, 1984.
6. C. F. F. Karney, Comparison of the Theory and the Practice of RF Current Drive, PPPL-2152, Plasma Physics Laboratory, Princeton University, 1984.
7. E. T. Gorbunov, S. V. Mirnov, and V. S. Strelkov, Nucl. Fusion 10, 43 (1970).
8. R. Goldston, Plasma Phys. Controlled Fusion 26, 87 (1984).
9. M. Murakami et al., Nucl. Fusion 16, 347 (1976).
10. S. N. Rosenwasser et al., J. Nucl. Mater. 122 & 123, 1107 (1984).
11. R. G. Perkins et al., "Compact Tokamak Hybrid Reactor Systems," in Proceedings of the 10th International Conference on Plasma Physics and Controlled Nuclear Fusion Research, London, September 1984, paper IAEA-CN-44/H-I-4.
12. J. A. Schmidt et al., "The Tokamak Fusion Core Experiment Studies," in Proceedings of the 10th International Conference on Plasma Physics and Controlled Nuclear Fusion Research, London, September 1984, paper IAEA-CN-44/H-I-3.
13. E. C. Selcow, Fusion Engineering Design Center Physics Systems Code, to be published.
14. W. A. Houlberg et al., "Contour Analysis of Fusion Reactor Performance," Nucl. Fusion 22, 935 (1982).

15. C. S. Chang and F. L. Hinton, Phys. Fluids 25, 1493 (1982).

16. R. L. Reid et al., The Tokamak Systems Code, ORNL/FEDC-84/9, Oak Ridge National Laboratory, March 1985.

17. T. H. Jensen and M. S. Chu, Current Drive and Helicity Injection, GA-A17424, GA Technologies, November 1983.

18. P. M. Bellan, Phys. Fluids 27, 2191 (1984).

19. W. R. Hamilton and K. E. Rothe, Fusion Technol. 8, 356 (1985).

ORNL/FEDC-85/5
Dist. Category UC-20 c,d

INTERNAL DISTRIBUTION

1. R. J. Barrett
2. D. B. Batchelor
3. D. D. Bates
4. C. O. Beasley
5. W. R. Becraft
6. D. T. Blackfield
7. T. G. Brown
8. R. D. Burris
9. C. E. Bush
10. B. A. Carreras
11. R. E. Clausing
12. R. J. Colchin
13. W. A. Cooper
14. E. C. Crume
15. R. A. Dory
16. J. L. Dunlap
17. G. R. Dyer
18. P. H. Edmonds
19. A. C. England
20. W. A. Gabbard
21. J. D. Galambos
22. L. Garcia
23. J. C. Glowienka
24. G. E. Gorker
25. J. H. Harris
26. H. H. Haselton
27. D. E. Hastings
28. C. L. Hedrick
29. D. L. Hillis
30. S. P. Hirshman
31. J. T. Hogan
32. W. A. Houlberg
33. H. C. Howe
34. R. C. Isler
35. E. F. Jaeger
36. T. C. Jernigan
37. S. S. Kalsi
38. P. W. King
39. R. A. Langley
40. E. A. Lazarus
41. V. D. Lee
42. D. C. Lousteau
43. M. S. Lubell
44. J. F. Lyon
45. C. H. Ma
46. J. B. Miller
47. S. L. Milora
48. P. K. Mioduszewski
49. M. Murakami
50. G. H. Neilson
51. W. D. Nelson
52. V. K. Pare
53–57. Y-K. M. Peng
58. D. A. Rasmussen
59. R. L. Reid
60. R. K. Richards
61. B. W. Riemer
62. E. Rodriguez-Solano
63. J. A. Rome
64. M. J. Saltmarsh
65. E. C. Selcow
66. K. C. Shaing
67. T. E. Shannon
68. J. Sheffield
69. D. J. Sigmar
70. P. T. Spampinato
71. D. A. Spong
72. W. L. Stirling
73. D. J. Strickler
74. D. W. Swain
75. G. E. Taylor
76. C. C. Tsai
77. N. A. Uckan
78. J. W. Whealton
79. J. B. Wilgen
80. W. R. Wing
81. J. J. Yugo
82. R. A. Zuhr
83–84. Laboratory Records Department
85. Laboratory Records, ORNL-RC
86. Central Research Library
87. Document Reference Section
88. Fusion Energy Division Library
89. Fusion Energy Division Publications Office
90. ORNL Patent Office

EXTERNAL DISTRIBUTION

91. M. A. Abdou, Boelter Hall, University of California, Los Angeles, CA 90024
92. C. A. Anderson, Westinghouse Electric Corporation, Advanced Energy Energy Systems Division, P.O. Box 158, Madison, PA 15663
93. J. L. Anderson, CMB-3, Mail Stop 348, Los Alamos National Laboratory, P.O. Box 1633, Los Alamos, NM 87545
94. C. C. Baker, FPP/208, Argonne National Laboratory, 9700 South Cass Avenue, Argonne, IL 60439
95. D. S. Beard, Office of Fusion Energy, Office of Energy Research, ER-531 Germantown, U.S. Department of Energy, Washington, DC 20545
96. K. L. Black, Department E452, McDonnell Douglas Astronautics Company, P.O. Box 516, St. Louis, MO 63166
97. R. Botwin, C47-05, Grumman Aerospace Corporation, P.O. Box 31, Bethpage, NY 11714
98. W. B. Briggs, McDonnell Douglas Astronautics Company, P.O. Box 516, St. Louis, MO 63166
99. J. N. Brooks, FPP/207, Argonne National Laboratory, 9700 South Cass Avenue, Argonne, IL 60439
100. S. C. Burnett, GA Technologies, Inc., P.O. Box 81608, San Diego, CA 92138
101. J. D. Callen, Department of Nuclear Engineering, University of Wisconsin, Madison, WI 53706
102. R. N. Cherdack, Burns and Roe, Inc., 800 Kinderkamack Road, Oradell, NJ 07649
103. D. R. Cohn, MIT Plasma Fusion Center, 167 Albany Street, Cambridge, MA 02139
104. J. W. Coursen, C36-05, Grumman Aerospace Corporation, P.O. Box 31, Bethpage, NY 11714
105. R. W. Conn, School of Chemical, Nuclear, and Thermal Engineering, Boelter Hall, University of California, Los Angeles, CA 90024
106. J. G. Crocker, EG&G Idaho, P.O. Box 1625, Idaho Falls, ID 83401
107. G. R. Dalton, Department of Nuclear Engineering Science, Nuclear Science Center, University of Florida, Gainesville, FL 32611
108. R. C. Davidson, Massachusetts Institute of Technology, 77 Massachusetts Avenue, Cambridge, MA 02139
109. N. A. Davies, Office of Fusion Energy, Office of Energy Research, ER-51 Germantown, U.S. Department of Energy, Washington, DC 20545
110. S. O. Dean, Director, Fusion Energy Development, Science Applications International Corporation, 2 Professional Drive, Suite 249, Gaithersburg, MD 20760
111. D. DeFreece, E451, Building 81/1/B7, McDonnell Douglas Astronautics Company, P.O. Box 516, St. Louis, MO 63166
112. J. N. Doggett, L-441, Lawrence Livermore National Laboratory, P.O. Box 5511, Livermore, CA 94550
113. H. Dreicer, Division Leader, CRT, Los Alamos National Laboratory, P.O. Box 1663, Los Alamos, NM 87545
114. D. Ehst, Argonne National Laboratory, 9700 South Cass Avenue, Argonne, IL 60439
115. F. Farfaletti-Casali, Engineering Division, Joint Research Center, Ispra Establishment, 21020 Ispra (Varese), Italy
116. P. A. Finn, Fusion Power Program, Argonne National Laboratory, 9700 South Cass Avenue, Argonne, IL 60439
117. H. K. Forsen, Bechtel Group, Inc., Research & Engineering, P.O. Box 3965, San Francisco, CA 94119
118. J. S. Foster, Jr., Building R4-2004, TRW Defense and Space Systems, 1 Space Park, Redondo Beach, CA 90278

119. T. K. Fowler, Associate Director for Magnetic Fusion Energy, L-436, Lawrence Livermore National Laboratory, P.O. Box 5511, Livermore, CA 94550
120. J. W. French, Princeton Plasma Physics Laboratory, P.O. Box 451, Princeton, NJ 08544
121. H. P. Furth, Director, Princeton Plasma Physics Laboratory, P.O. Box 451, Princeton, NJ 08544
122. J. G. Gavin, Jr., President, A01-11, Grumman Aerospace Corporation, P.O. Box 31, Bethpage, NY 11714
123. S. K. Ghose, Lawrence Livermore National Laboratory, P.O. Box 5511, Livermore, CA 94550
124. G. Gibson, Westinghouse Electric Corporation, Fusion Power Systems Department, P.O. Box 10864, Pittsburgh, PA 15236
125. J. R. Gilleland, Manager, Fusion Project, GA Technologies, Inc., P.O. Box 81608, San Diego, CA 92138
126. M. Y. Gohar, Argonne National Laboratory, 9700 South Cass Avenue, Argonne, IL 60439
127. R. W. Gould, Department of Applied Physics, California Institute of Technology, Pasadena, CA 91109
128. M. W. Griffin, Department E236, McDonnell Douglas Astronautics Company, P.O. Box 516, St. Louis, MO 63166
129. R. A. Gross, Plasma Research Laboratory, Columbia University, New York, NY 10027
130. J. R. Haines, McDonnell Douglas Astronautics Company, St. Louis, MO 63166
131. C. D. Henning, Lawrence Livermore National Laboratory, P.O. Box 5511, Livermore, CA 94550
132. J. J. Holmes, Westinghouse-Hanford Engineering Development Laboratory, P.O. Box 1970, Richland, WA 99352
133. D. Hwang, Princeton Plasma Physics Laboratory, P.O. Box 451, Princeton, NJ 08544
134. J. B. Joyce, Princeton Plasma Physics Laboratory, P.O. Box 451, Princeton, NJ 08544
135. R. A. Krakowski, CTR-12, Mail Stop 641, Los Alamos National Laboratory, P.O. Box 1663, Los Alamos, NM 87545
136. G. L. Kulcinski, University of Wisconsin, Department of Nuclear Engineering, Engineering Research Building, Room 439, 1500 Johnson Drive, Madison, WI 53706
137. D. L. Kummer, McDonnell Douglas Astronautics Company, P.O. Box 516, St. Louis, MO 63166
138. W. Marton, Office of Fusion Energy, Office of Energy Research, ER-55 Germantown, U.S. Department of Energy, Washington, DC 20545
139. L. G. Masson, EG&G Idaho, Idaho National Engineering Laboratory, P.O. Box 1625, Idaho Falls, ID 83401
140. D. M. Meade, Princeton Plasma Physics Laboratory, P.O. Box 451, Princeton, NJ 08544
141. A. T. Mense, Building 107, Post B2, McDonnell Douglas Astronautics Company, P.O. Box 516, St. Louis, MO 63166
142. R. W. Moir, Lawrence Livermore Laboratory, P.O. Box 5511, Livermore, CA 94550
143. D. B. Montgomery, MIT Plasma Fusion Center, 167 Albany Street, Cambridge, MA 02139
144. A. E. Munier, Grumman Aerospace Corporation, P.O. Box 31, Bethpage, NY 11714
145. R. E. Nygren, FPP/207, Argonne National Laboratory, 9700 South Cass Avenue, Argonne, IL 60439
146. T. Ohkawa, GA Technologies, Inc., P.O. Box 81608, San Diego, CA 92138
147. J. A. O'Toole, Plasma Physics Laboratory, James Forrestal Campus, Building I-P, Room 8A, P.O. Box 451, Princeton, NJ 08544
148. R. R. Parker, Francis Bitter National Magnet Laboratory, 170 Albany Street, Cambridge, MA 02139
149. B. Pease, Culham Laboratory, Abingdon, Oxfordshire OX14 3DB, United Kingdom
150. M. Pelovitz, Princeton Plasma Physics Laboratory, P.O. Box 451, Princeton, NJ 08544

151. F. W. Perkins, Princeton Plasma Physics Laboratory, P.O. Box 451, Princeton, NJ 08544
152. M. Porkolab, Massachusetts Institute of Technology, 77 Massachusetts Avenue, Cambridge, MA 02139
153. D. E. Post, Princeton Plasma Physics Laboratory, P.O. Box 451, Princeton, NJ 08544
154. R. E. Price, Office of Fusion Energy, Office of Energy Research, ER-55 Germantown, U.S. Department of Energy, Washington, DC 20545
155. F. A. Puhn, GA Technologies, Inc., P.O. Box 81608, San Diego, CA 92138
156. J. Purcell, GA Technologies, Inc., P.O. Box 81608, San Diego, CA 92138
157. R. V. Pyle, University of California, Lawrence Berkeley Laboratory, Berkeley, CA 94720
158. J. M. Rawls, GA Technologies, Inc., P.O. Box 81608, San Diego, CA 92138
159. M. Roberts, Office of Fusion Energy, ER-52 Germantown, U.S. Department of Energy, Washington, DC 20545
160. J. D. Rogers, Los Alamos National Laboratory, P.O. Box 1663, Los 158mos, NM 87545
161. M. L. Rogers, Monsanto Research Corporation, Mound Laboratory 159ility, P.O. Box 32, Miamisburg, OH 45342
162. M. N. Rosenbluth, RLM 11.218, Institute for Fusion Studies, University of Texas, Austin, TX 78712
163. P. H. Rutherford, Princeton Plasma Physics Laboratory, P.O. Box 451, Princeton, NJ 08544
164. J. A. Schmidt, Princeton Plasma Physics Laboratory, P.O. Box 451, Princeton, NJ 08544
165. J. Schultz, MIT Plasma Fusion Center, 167 Albany Street, Cambridge, MA 02139
166. F. R. Scott, Electric Power Research Institute, P.O. Box 10412, Palo Alto, CA 94304
167. G. Sheffield, Princeton Plasma Physics Laboratory, P.O. Box 451, Princeton, NJ 08544
168. D. Smith, Materials Science Division, Argonne National Laboratory, 9700 South Cass Avenue, Argonne, IL 60439
169. W. M. Stacey, Jr., Georgia Institute of Technology, School of Nuclear Engineering and Health Physics, Atlanta, GA 30332
170. D. Steiner, Rensselaer Polytechnic Institute, Nuclear Engineering Department, NES Building, Tibbets Avenue, Troy, NY 12181
171. E. Stern, Grumman Aerospace Corporation, CN-59, Forrestal Campus, Princeton, NJ 08544
172. P. M. Stone, Office of Fusion Energy, Office of Energy Research, ER-532 Germantown, U.S. Department of Energy, Washington, DC 20545
173. I. N. Sviatoslavsky, Room 33, Engineering Research Building, 1500 Johnson Drive, University of Wisconsin, Madison, WI 53706
174. R. E. Tatro, Manager, Energy Systems, M.Z. 16-1070, General Dynamics-Convair Division, P.O. Box 80847, San Diego, CA 92138
175. F. Thomas, B-20-5, Grumman Aerospace Corporation, Bethpage, NY 11714
176. K. I. Thomassen, Lawrence Livermore National Laboratory, P.O. Box 5511, Livermore, CA 94550
177. R. J. Thome, Francis Bitter National Magnet Laboratory, 170 Albany Street, Cambridge, MA 02139
178. C. Trachsel, McDonnell Douglas Astronautics Company, P.O. Box 516, St. Louis, MO 63166
179. A. W. Trivelpiece, Office of Energy Research, U.S. Department of Energy, Washington, DC 20545
180. L. R. Turner, Fusion Power Program, Argonne National Laboratory, 9700 South Cass Avenue, Argonne, IL 60439
181. E. H. Valeo, Princeton Plasma Physics Laboratory, P.O. Box 451, Princeton, NJ 08544
182. R. Varma, Physical Research Laboratory, Navrangpura, Ahmedabad 380009, India
183. K. E. Wakefield, Princeton Plasma Physics Laboratory, P.O. Box 451, Princeton, NJ 08544
184. J. C. Wesley, GA Technologies, Inc., P.O. Box 81608, San Diego, CA 92138

185. J. E. C. Williams, Francis Bitter National Magnet Laboratory, 170 Albany Street, Cambridge, MA 02139
186. H. H. Yoshikawa, W/A-62, Hanford Engineering Development Laboratory, P.O. Box 1970, Richland, WA 99352
187. K. M. Young, Princeton Plasma Physics Laboratory, P.O. Box 451, Princeton, NJ 08544
188. N. E. Young, Princeton Plasma Physics Laboratory, P.O. Box 451, Princeton, NJ 08544
189. Bibliothek, Max-Planck Institut fur Plasmaphysik, D-8046 Garching, Federal Republic of Germany
190. Bibliothek, Institut fur Plasmaphysik, KFA, Postfach 1913, D-5170 Julich, Federal Republic of Germany
191. Bibliotheque, Service du Confinement des Plasmas, CEA, B.P. No. 6, 92 Fontenay-aux-Roses (Seine), France
192. Documentation S.I.G.N., Department de la Physique du Plasma et de la Fusion Controlee, Association EURATOM-CEA, Centre d'Etudes Nucleaires, B.P. 85, Centre du Tri, 38041 Grenoble, Cedex, France
193. Library, Centre de Recherches en Physique des Plasmas, 21 Avenue des Bains, 1007 Lausanne, Switzerland
194. Library, Culham Laboratory, UKAEA, Abingdon, Oxfordshire, OX14 3DB, England
195. Library, FOM Instituut voor Plasma-Fysica, Rijnhuizen, Edisonbaan 14, 3439 MN Nieuwegein, Netherlands
196. Library, Institute of Physics, Academia Sinica, Beijing, People's Republic of China
197. Library, Institute for Plasma Physics, Nagoya University, Nagoya 464, Japan
198. Library, International Centre for Theoretical Physics, Trieste, Italy
199. Library, JET Joint Undertaking, Abingdon, Oxfordshire, OX14 3DB, England
200. Library, Laboratorio Gas Ionizzati, CP 56, I-00044 Frascati, Rome, Italy
201. Plasma Research Laboratory, Australian National Laboratory, P.O. Box 4, Canberra, ACT 2000, Australia
202. Thermonuclear Library, Japan Atomic Energy Research Institute, Tokai, Naka, Ibaraki, Japan
203. Library, Plasma Physics Laboratory, Kyoto University, Gokasho, Uji, Kyoto, Japan
204. Office of the Assistant Manager for Energy Research and Development, U.S. Department of Energy, Oak Ridge Operations, P.O. Box E, Oak Ridge, TN 37831

205–381. Given distribution as shown in TIC-4500, Magnetic Fusion Energy (Distribution Category UC-20 c,d: Reactor Materials and Fusion Systems)